13-Park, Kim, Jung - 2013 - Origin of Selective Guest-Induced Magnetism Transition in FeMOF-74

DATASET · JULY 2014

THE JOURNAL OF PHYSICAL CHEMISTRY Letters

Letter

pubs.acs.org/JPCL

Origin of Selective Guest-Induced Magnetism Transition in Fe/MOF-74

Joonho Park,† Heejin Kim,† and Yousung Jung*

Graduate School of Energy, Environment, Water and Sustainability (EEWS), Korea Advanced Institute of Science and Technology, Daejeon, 305-701, Republic of Korea

Supporting Information

ABSTRACT: The experimentally observed selective guest-induced (olefin-induced) magnetism transition from ferromagnetism (FM) to antiferromagnetism (AFM) on Fe/MOF-74 is investigated using the first principles calculations. We reveal that FM in bare MOF is due to direct exchange interaction between neighboring Fe ions while the olefin-adsorbed MOF prefers AFM through the superexchange interaction. We find that geometrical changes (such as Fe−Fe distance and Fe−O−Fe angle) associated with strong interaction of olefin π-bonds with open metal sites in MOF framework define magnetic coupling while electronic effects such as charge transfer and orbital interaction play a minor role. Additionally, the weak interchain magnetic coupling whose magnitude is smaller than the intrachain coupling by an order of magnitude can be switched by introducing a paramagnetic ligand between metal atoms. This work offers the origin of magnetism in MOFs with open metal sites and its subtle alteration due to selective guest binding that can be used for future design of lightweight porous magnet and magnetic separation of oxygen.

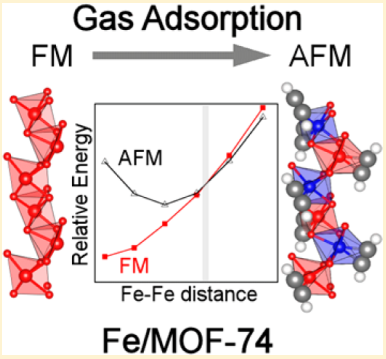

SECTION: Molecular Structure, Quantum Chemistry, and General Theory

The metal−organic framework (MOF) is composed of inorganic strut and organic linker, which make its functionality extremely diverse by tuning the metal centers and functional groups.[1] This modifiability and high surface areas due to the pores that range from a few angstroms to several nanometers enable MOFs to be applicable in the gas manipulation such as carbon capture,[2−7] hydrogen storage,[8−10] acetylene storage,[11] and methane storage.[12,13] Recently, light hydrocarbon separation has appeared for a new application of MOFs[14−17] in the petrochemical industry for lowering the energy costs of currently used cryogenic distillation technology.[18] Among several candidates, Fe/MOF-74 showed an outstanding selectivity for olefin compared to paraffin due to the strong π-complexation with the open metal sites. During the latter hydrocarbon separation measurements, Fe/MOF-74 also exhibited an intriguing magnetism phenomenon where the adsorption of olefin molecules changed the ferromagnetic (FM) state along the one-dimensional (1D) chain of the MOF framework to the antiferromagnetic (AFM) state, although the adsorption of paraffin molecules did not show the same effects.[15] The bare Fe/MOF-74 (or CPO27-Fe) is constructed from the infinite helical building units of $Fe^{2+}O_5$ polyhedron that gives an FM coupling along the chain, and 2,5-dioxido-1,4-benzene-dicarboxylate (DOBDC) organic linkers that give an AFM coupling between chains as shown in Figure 1.

While several changes in magnetic properties induced by guests have been reported in MOFs, such as the change of critical ordering temperature (T_c),[19,20] spin crossover between high spin and low spin,[21,22] and FM−AFM transition in the solvent,[23−26] the magnetic transition from FM to AFM through gas adsorption is quite unique in MOF-74. This kind of magnetism transition has become a critical issue in the application field of lightweight magnet, magnetic sensors, and magnetic separation media.[26,27] In fact, magnetic MOFs of this kind have been contemplated for oxygen separation (magnetic separation) for quite some time, and understanding the

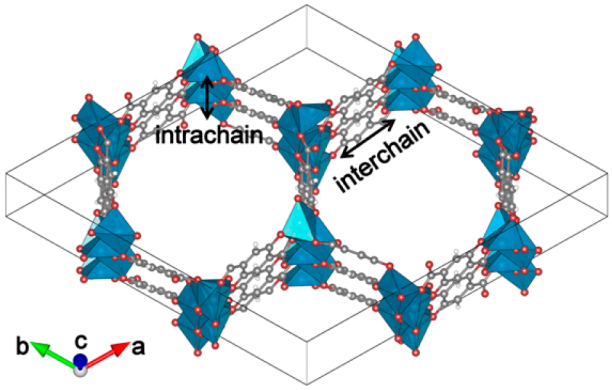

Figure 1. Crystal structure of bare Fe/MOF-74. Blue, red, gray, and white are Fe, O, C, and H, respectively.

Received: July 17, 2013
Accepted: July 19, 2013

   dx.doi.org/10.1021/jz4015103 | J. Phys. Chem. Lett. 2013, 4, 2530−2534

underlying origin of the magnetism transition in Fe/MOF-74 would be a first step in that direction.

Herein, we report the origin of the selective magnetism transition in Fe/MOF-74 for the hydrocarbons adsorption using the periodic density functional theory (DFT) calculations.[28] We used supercells containing 36 adsorption sites that can fully describe the intrachain and interchain magnetic couplings as shown in Figure 1. More detailed calculation methods are presented in the Supporting Information (SI).[29−32]

In our notation of magnetic coupling, we will use the intrachain coupling as a first index and the interchain coupling as a second index. For clear representation, the interchain magnetic coupling will be denoted as "par" for parallel alignment or "anti" for antiparallel alignment (Figure 2). In other words, the bare Fe/MOF-74 has an FM/anti coupling for the intra/interchain array of Fe atoms (Figure 2a). In experiments, the magnetic structure of the paraffin adsorbed Fe/MOF-74 is identical to that of bare Fe/MOF-74, while an olefin adsorption inverts the intrachain coupling from FM to the AFM with the interchain coupling remaining antiparallel, making the AFM/anti coupling (Figure 2b) the ground state for olefin-adsorbed Fe/MOF-74.

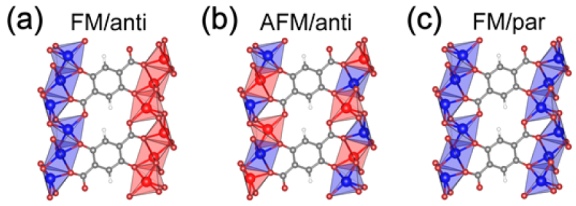

Figure 2. Three different magnetic orderings along the inter/intrachain considered in this work. Blue and red Fe-polyhedra indicate the up- or down-spin states, respectively. In the present case, (a) FM/anti corresponds to the magnetic states for bare MOF and MOF-paraffin complex, (b) AFM/anti corresponds to MOF-olefin complex, and (c) FM/par corresponds to permanent MOF magnet.

To understand first the intrachain FM coupling of the bare Fe/MOF-74, relative energies of AFM/anti (intrachain AFM) and FM/anti (intrachain FM) couplings were evaluated with varying the Fe−Fe distance from 2.79 Å to 3.31 Å (Figure 3a). The Fe−Fe distance of 2.79 and 3.31 Å are taken from the fully optimized geometry of bare MOF in FM/anti coupling and acetylene adsorbed MOF in AFM/anti coupling, i.e., in each ground state. By using these geometries as two end members, the initial geometries of intermediate states are obtained by linear interpolation. Then all geometries including intermediates and two end members were fully optimized with fixing the Fe−Fe distance. Remarkably, the FM/anti → AFM/anti transition (a→b in Figure 2) is observed in the bare Fe/MOF-74 when the Fe−Fe distance is gradually tuned, even in the absence of guest molecules, as marked with a vertical dotted line in Figure 3a.

The projected densities of states (DOS) of d-orbital of Fe ion are drawn for different structures and magnetism in Figure 3b, where the top and bottom sides are for the up- and down-spins, respectively. One down-spin electron in d^6 of Fe^{2+} ion is located just below the Fermi level, so it is the highest occupied molecular orbital (HOMO) whose electron density isosurfaces are also drawn in the inset. At an equilibrium Fe−Fe distance (2.79 Å) of bare Fe/MOF-74, direct orbital interactions between Fe ions occur, and the subsequent level splitting

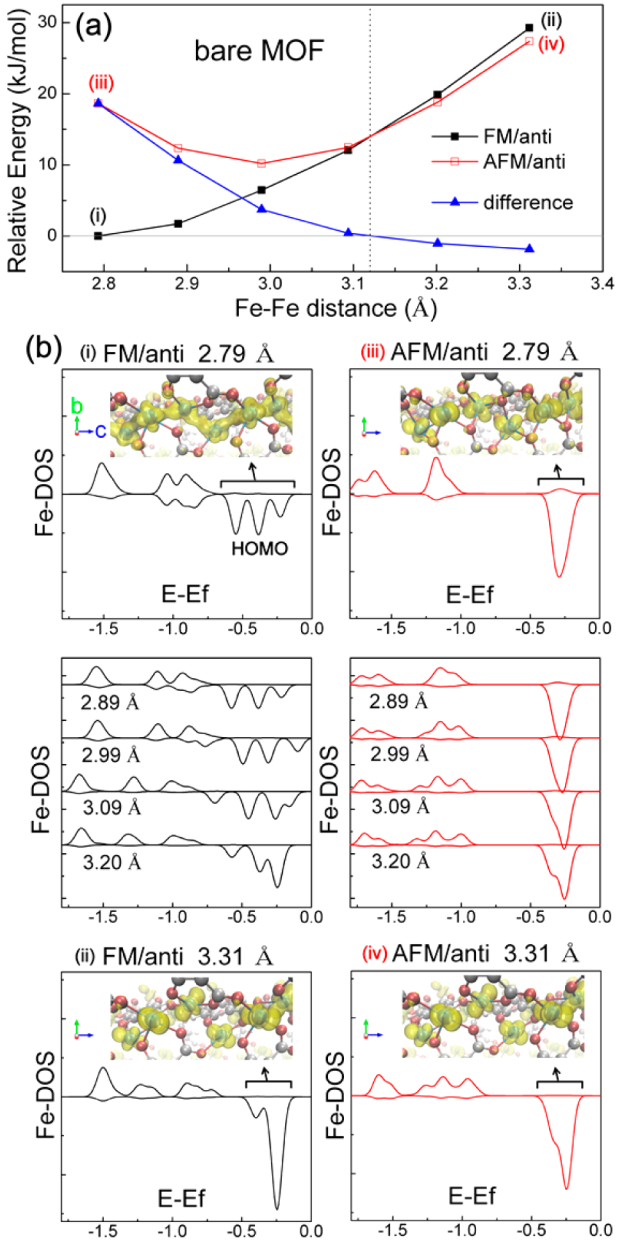

Figure 3. (a) The relative energies of FM/anti and AFM/anti ordering and their difference (blue) for bare Fe/MOF-74 as a function of Fe−Fe distance. The bare MOF can undergo intrachain FM-to-AFM transition at elongated Fe−Fe distance 3.12 Å, even without gas adsorption. (b) The DOS of Fe atom and electron density isosurfaces at the HOMO for each magnetic ordering and Fe−Fe distance ((i)−(iv)). Blue, red, and gray spheres are Fe, O, and C, respectively. All data for intermediate states are presented in Figure S2 in the SI.

appears in the FM/anti state (Figure 3b(i)). The orbital plot visually indicates that the HOMO electrons of neighboring Fe ions interact significantly with each other not mediated oxygen suggesting a direct interaction between adjacent Fe ions, which is not found in all other cases (Figure 3b(ii),(iii),(iv)). At the same Fe−Fe distance but when the FM/anti state is switched to AFM/anti, the band splitting does not appear (Figure 3b(iii)), and the electron densities are more localized. The super-exchange interaction between Fe ions through the edge-sharing oxygen can also contribute to the magnetic coupling, but it is relatively negligible at this distance (2.79 Å) since the Fe−O−Fe bond angle is 83.9° in the bare Fe/MOF-74.[33,34]

dx.doi.org/10.1021/jz4015103 | J. Phys. Chem. Lett. 2013, 4, 2530−2534

Consistently, the HOMO is composed mainly of 3d electrons of Fe, and there is not much overlap with oxygen to allow superexchange coupling (Figure S1 in the SI).

These phenomena hold up to the Fe−Fe distance of ∼3.12 Å, the crossover point between the FM/anti and AFM/anti couplings. While the HOMO electrons of Fe ions are able to interact with each other at a distance range of 2.79−3.12 Å as evidenced by the splitting of the HOMO levels, the energy gain arising from the mixing of the filled levels and spin-pairing seems to be not much greater than the favorable exchange interactions (K) between the parallel spins. Note that the experimental Fe−Fe distance[15] (2.99 Å) is within this range and the direct interaction also appears at 2.99 Å for the FM/anti coupling (Figure 3b). Beyond the crossover point, two magnetic couplings become quite degenerate since the Fe−Fe distance is too far for direct interactions (for both orbital mixing and exchange interactions). Instead, the slight stabilization for the AFM/anti coupling is observed that is now due to the superexchange interaction via the Fe−O−Fe pathway since the Fe−O−Fe bond angle increases to ∼107° at a Fe−Fe distance of 3.31 Å (compared to 83.9° at Fe−Fe distance of 2.79 Å), which can allow superexchange coupling. We note that the Goodenough−Kanamori rule supports strong AFM coupling as the Fe−O−Fe bond angle widens up and approaches 180°.[33,34] Therefore, we can conclude that the intrachain FM coupling in the bare Fe/MOF-74 at equilibrium Fe−Fe distance is due to the direct exchange interaction at the HOMO level that is mainly composed of Fe-3d electrons.

Figure 4a next shows the calculated energy difference between AFM/anti and FM/anti coupling for various hydrocarbons adsorption, i.e., the guest-dependent intrachain magnetism transition energy, where the positive values mean that the intrachain FM coupling is more stable than the intrachain AFM coupling. The stability of intrachain FM coupling in the bare Fe/MOF-74 (8.34 kJ/mol) becomes weaker as the strength of the gas binding gets larger, and eventually the intrachain AFM state becomes more stable for the olefins adsorbed Fe/MOF-74. This olefin/paraffin selective magnetism transition and the order of FM stability, bare > Ma > Ea > Pa > Py > Ey > Ay, are completely consistent with the experimental isosteric heats of adsorption measurements.[15] Similarly, the calculated intrachain magnetism transition energy is in good agreement with the trend of magnetic coupling constants estimated in experiments.[15]

On the basis of the previous potential energy scan for the bare Fe/MOF-74 in Figure 3, the intrachain magnetic behavior of Fe/MOF-74 can be considered as a competition between FM coupling that is attributed to the Fe−Fe direct orbital interactions and the AFM coupling that arises mainly from the Fe−O−Fe superexchange interactions associated with the geometric change of the framework. The interacting guest molecules can affect the intrachain magnetic couplings as follows:

(1) The interacting gas molecules weaken the direct interaction between Fe atoms (the source of intrachain FM coupling) by attracting the 3d electrons from the Fe−Fe interacting orbital and consequently elongating the Fe−Fe distances.

(2) The interacting gas molecules strengthen the superexchange interaction between Fe atoms through oxygen bridge (the source of intrachain AFM coupling) by increasing the Fe−O−Fe angles.

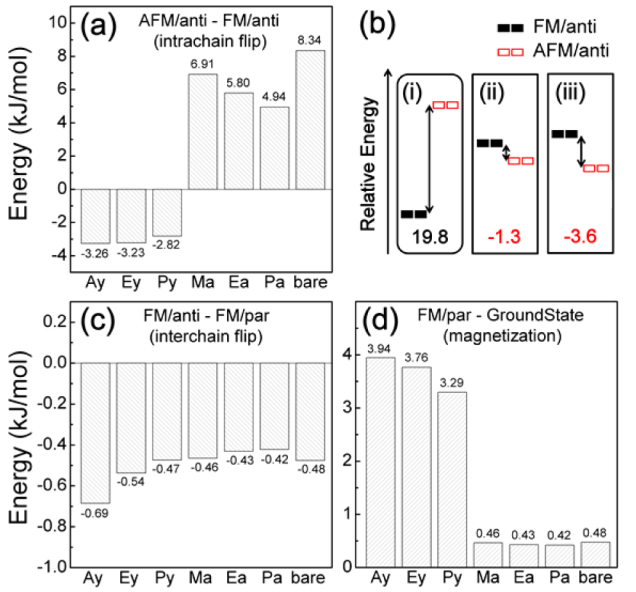

Figure 4. (a) The intrachain spin-flip energy, namely, the energy required to flip spins along the 1D chain from FM to AFM. The strong FM coupling in bare Fe/MOF-74 is diminished when the strongly interacting gases are adsorbed. Ay, Ey, Py, Ma, Ea, and Pa are acetylene, ethylene, propylene, methane, ethane, and propane, respectively. (b) The relative energy differences between FM/anti and AFM/anti orderings in the (i) bare MOF, (ii) Ay-adsorbed MOF without Ay molecules, and (iii) Ay-adsorbed MOF. The intrachain spin-flip is primarily due to the structural changes of the MOF framework. This result is fully consistent with Figure 3a. (c) The interchain spin-flip energy, namely, the energy required to flip spins across the 1D chains from "par" to "anti". (d) The magnetization energy defined as a difference between the lowest energy spin state and magnetized (FM/par, Figure 2c) state.

Therefore, the more strongly interacting gas molecules stabilize the AFM coupling to a greater extent along the intrachain direction. To be more specific, the factors affecting the magnetic coupling can be divided into the geometric effect from the host structure and the additional electronic effect from the guest molecules. To identify these two effects on the magnetic behavior, we compared the relative stability of AFM/anti and FM/anti couplings in the fixed geometry of (i) the fully optimized bare MOF, (ii) MOF host only whose geometry is extracted from the fully optimized Ay-adsorbed MOF, and (iii) fully optimized Ay-adsorbed MOF (Figure 4b). Energetic change in (i) → (ii) is the measure of geometric effect of the host framework for the observed magnetism transition while the change in (ii) → (iii) is responsible for the electronic effect from the guest.

In bare Fe/MOF-74, AFM/anti is less stable than FM/anti by 19.8 kJ/mol. However, in the Ay-adsorbed Fe/MOF-74 structure without Ay molecules (distorted MOF to accommodate the guest molecules), AFM/anti is already more stable than FM/anti by 1.3 kJ/mol, indicating that the structural evolution stabilizes the intrachain AFM coupling significantly by 21.1 kJ/mol. In the subsequent complexation with the gas (Ay), AFM/anti is further stabilized, but only by 2.3 kJ/mol by the additional electronic effects such as charge transfer and orbital interactions. In this step, the increased charge in Fe ion due to the forward charge donation from Ay to the open metals makes the net spin moment of Fe decrease from 3.61 to 3.56. Therefore, we can conclude that the adsorption-induced

dx.doi.org/10.1021/jz4015103 | J. Phys. Chem. Lett. 2013, 4, 2530−2534

intrachain magnetic transition of Fe/MOF-74 is mainly due to the guest-dependent geometry changes of the framework such as Fe−Fe distances and Fe−O−Fe angles, with minor electronic effects, consistent with the fact that the magnetism is a subtle result of the overlap of electrons.

In contrast to the intrachain coupling, the interchain interactions are consistently antiparallel regardless of the guest molecules (Figure 4c). Besides, comparison of the calculated intrachain (Figure 4a) versus interchain (Figure 4c) magnetic transition energy indicates that the intrachain coupling is significantly stronger than the interchain coupling by an order of magnitude in Fe/MOF-74, consistent with a recent report.[35] As a result, the energy required for magnetization of olefin-adsorbed Fe/MOF-74, which needs a intrachain spin-flip, is higher than that of paraffin-adsorbed Fe/MOF-74, which needs a interchain spin-flip for the magnetization (Figure 4d), consistent with the magnetic susceptibility measurement of Bloch et al.[15] The origin of long-range interchain AFM coupling (7.58 Å) across the aromatic linker is expected to be understood by a superexchange interaction, and it can be changed into parallel alignment when the present nonmagnetic ligand is replaced by a paramagnetic ligand.[36] Indeed, when we hypothetically remove one hydrogen atom from a benzene ring to form a radical in the organic linker, the interchain parallel coupling (FM/par) became more stable than FM/anti coupling by 0.71 kJ/mol in bare Fe/MOF-74. In such a case, the interchain Fe atoms align parallel through the opposite spin of a radical, resulting in the permanent magnet since the magnetic moments are different for Fe^{2+} ($S = 2$) and radical ($S = -1/2$).

In summary, we revealed the origin of FM coupling along the 1D chain of Fe/MOF-74 and its selective guest-dependent transition to the AFM coupling. We find that the intrachain magnetic transition observed upon olefin adsorption is an intriguing result of the competition between the FM coupling originated from the Fe−Fe direct exchange interaction and the AFM coupling due to the Fe−O−Fe indirect (superexchange) interaction. The olefin adsorption turns out to diminish the Fe−Fe direct interaction by pulling out Fe atoms. We show that this magnetic transition is mainly due to the geometry changes of the MOF framework upon the π-complexation with olefin that strengthens the Fe−O−Fe superexchange interactions, rather than minor electronic effects such as charge transfer between the framework and the guest. The present understandings would be helpful for designing the microporous magnet and sensors for recognizing small molecules such as in magnetic separation of oxygen.

■ ASSOCIATED CONTENT

Supporting Information

Calculation details, DOS of Fe and O atoms, PDOS of Fe, and electron density isosurfaces as a function of Fe−Fe distance. This material is available free of charge via the Internet at http://pubs.acs.org.

■ AUTHOR INFORMATION

Corresponding Author

*E-mail: ysjn@kaist.ac.kr.

Author Contributions

†These authors contributed equally.

Notes

The authors declare no competing financial interest.

■ ACKNOWLEDGMENTS

We acknowledge the support from the Korea CCS R&D Center, Basic Science Research (2010-0023018), and the WCU program (R31-2008-000-10055-0) funded by the Ministry of Education, Science and Technology of the Korean government, as well as the KAIST EEWS Initiative. We are grateful to Profs. Omar Yaghi and Yong-Hyun Kim for helpful discussions. Generous computing time from KISTI is gratefully acknowledged.

■ REFERENCES

(1) Rosi, N. L.; Kim, J.; Eddaoudi, M.; Chen, B.; O'Keeffe, M.; Yaghi, O. M. Rod Packings and Metal−Organic Frameworks Constructed from Rod-Shaped Secondary Building Units. *J. Am. Chem. Soc.* **2005**, *127*, 1504−1518.

(2) Park, J.; Kim, H.; Han, S. S.; Jung, Y. Tuning Metal−Organic Frameworks with Open-Metal Sites and Its Origin for Enhancing CO_2 Affinity by Metal Substitution. *J. Phys. Chem. Lett.* **2012**, *3*, 826−829.

(3) Sumida, K.; Rogow, D. L.; Mason, J. A.; McDonald, T. M.; Bloch, E. D.; Herm, Z. R.; Bae, T.-H.; Long, J. R. Carbon Dioxide Capture in Metal−Organic Frameworks. *Chem. Rev.* **2012**, *112*, 724−781.

(4) Wilmer, C. E.; Snurr, R. Q. Towards Rapid Computational Screening of Metal−Organic Frameworks for Carbon Dioxide Capture: Calculation of Framework Charges via Charge Equilibration. *Chem. Eng. J.* **2010**, *171*, 775−781.

(5) Wu, H.; Simmons, J. M.; Srinivas, G.; Zhou, W.; Yildirim, T. Adsorption Sites and Binding Nature of CO_2 in Prototypical Metal−Organic Frameworks: A Combined Neutron Diffraction and First-Principles Study. *J. Phys. Chem. Lett.* **2010**, *1*, 1946−1951.

(6) Yazaydin, A. O.; et al. Screening of Metal−Organic Frameworks for Carbon Dioxide Capture from Flue Gas Using a Combined Experimental and Modeling Approach. *J. Am. Chem. Soc.* **2009**, *131*, 18198−18199.

(7) Han, S. S.; Kim, D.; Jung, D. H.; Cho, S.; Choi, S.-h.; Jung, Y. Accurate Ab Initio-Based Force Field for Predictive CO_2 Uptake Simulations in MOFs and ZIFs: Development and Applications for MTV-MOFs. *J. Phys. Chem. C* **2012**, *116*, 20254−20261.

(8) Kim, Y.-H.; Sun, Y. Y.; Choi, W. I.; Kang, J.; Zhang, S. B. Enhanced Dihydrogen Adsorption in Symmetry-Lowered Metal-Porphyrin-Containing Frameworks. *Phys. Chem. Chem. Phys.* **2009**, *11*, 11400−11403.

(9) Rosi, N. L.; Eckert, J.; Eddaoudi, M.; Vodak, D. T.; Kim, J.; O'Keeffe, M.; Yaghi, O. M. Hydrogen Storage in Microporous Metal−Organic Frameworks. *Science* **2003**, *300*, 1127−1129.

(10) Zhou, W.; Wu, H.; Yildirim, T. Enhanced H_2 Adsorption in Isostructural Metal-Organic Frameworks with Open Metal Sites: Strong Dependence of the Binding Strength on Metal Ions. *J. Am. Chem. Soc.* **2008**, *130*, 15268−15269.

(11) Xiang, S.; Zhou, W.; Zhang, Z.; Green, M. A.; Liu, Y.; Chen, B. Open Metal Sites Within Isostructural Metal-Organic Frameworks for Differential Recognition of Acetylene and Extraordinarily High Acetylene Storage Capacity at Room Temperature. *Angew. Chem., Int. Ed.* **2010**, *49*, 4615−4618.

(12) Eddaoudi, M.; Kim, J.; Rosi, N.; Vodak, D.; Wachter, J.; O'Keeffe, M.; Yaghi, O. M. Systematic Design of Pore Size and Functionality in Isoreticular MOFs and Their Application in Methane Storage. *Science* **2002**, *295*, 469−72.

(13) Guo, Z.; et al. A Metal−Organic Framework with Optimized Open Metal Sites and Pore Spaces for High Methane Storage at Room Temperature. *Angew. Chem., Int. Ed.* **2011**, *50*, 3178−3181.

(14) Bae, Y.-S.; Lee, C. Y.; Kim, K. C.; Farha, O. K.; Nickias, P.; Hupp, J. T.; Nguyen, S. T.; Snurr, R. Q. High Propene/Propane Selectivity in Isostructural Metal-organic Frameworks with High Densities of Open Metal Sites. *Angew. Chem., Int. Ed.* **2012**, *51*, 1857−60.

(15) Bloch, E. D.; Queen, W. L.; Krishna, R.; Zadrozny, J. M.; Brown, C. M.; Long, J. R. Hydrocarbon Separations in a Metal-Organic

Framework with Open Iron(II) Coordination Sites. *Science* **2012**, *335*, 1606−1610.
(16) He, Y.; Krishna, R.; Chen, B. Metal−Organic Frameworks with Potential for Energy-Efficient Adsorptive Separation of Light Hydrocarbons. *Energy Environ. Sci.* **2012**, *5*, 9107−9120.
(17) Nijem, N.; Wu, H.; Canepa, P.; Marti, A.; Balkus, K. J.; Thonhauser, T.; Li, J.; Chabal, Y. J. Tuning the Gate Opening Pressure of Metal-Organic Frameworks (MOFs) for the Selective Separation of Hydrocarbons. *J. Am. Chem. Soc.* **2012**, *134*, 15201−15204.
(18) Eldridge, R. B. Olefin/Paraffin Separation Techonology: A Review. *Ind. Eng. Chem. Res.* **1993**, *32*, 2208−2212.
(19) Kaneko, W.; Ohba, M.; Kitagawa, S. A Flexible Coordination Polymer Crystal Providing Reversible Structural and Magnetic Conversions. *J. Am. Chem. Soc.* **2007**, *129*, 13706−13712.
(20) Navarro, J. A. R.; Barea, E.; Rodríguez-Diéguez, A.; Salas, J. M.; Ania, C. O.; Parra, J. B.; Masciocchi, N.; Galli, S.; Sironi, A. Guest-Induced Modification of a Magnetically Active Ultramicroporous, Gismondine-like, Copper(II) Coordination Network. *J. Am. Chem. Soc.* **2008**, *130*, 3978−3984.
(21) Halder, G. J.; Kepert, C. J.; Moubaraki, B.; Murray, K. S.; Cashion, J. D. Guest-Dependent Spin Crossover in a Nanoporous Molecular Framework Material. *Science* **2002**, *298*, 1762−1765.
(22) Ohba, M.; et al. Bidirectional Chemo-Switching of Spin State in a Microporous Framework. *Angew. Chem., Int. Ed.* **2009**, *48*, 4767−4771.
(23) Kurmoo, M.; Kumagai, H.; Chapman, K. W.; Kepert, C. J. Reversible Ferromagnetic−Antiferromagnetic Transformation upon Dehydration−Hydration of the Nanoporous Coordination Framework, $[Co_3(OH)_2(C_4O_4)_2]_3H_2O$. *Chem. Commun.* **2005**, 3012−3014.
(24) Motokawa, N.; Matsunaga, S.; Takaishi, S.; Miyasaka, H.; Yamashita, M.; Dunbar, K. R. Reversible Magnetism Between an Antiferromagnet and a Ferromagnet Related to Solvation/Desolvation in a Robust Layered $[Ru_2]_2TCNQ$ Charge-Transfer System. *J. Am. Chem. Soc.* **2010**, *132*, 11943−11951.
(25) Sun, W.-W.; Tian, C.-Y.; Jing, X.-H.; Wang, Y.-Q.; Gao, E.-Q. Solvent-Modulated Metamagnetism in a Nickel(II) Coordination Polymer with Mixed Azide and Carboxylate Bridges. *Chem. Commun.* **2009**, 4741−4743.
(26) Wriedt, M.; Yakovenko, A. A.; Halder, G. J.; Prosvirin, A. V.; Dunbar, K. R.; Zhou, H.-C. J. Reversible Switching from Antiferro- to Ferromagnetic Behavior by Solvent-Mediated, Thermally-Induced Phase Transitions in a Trimorphic MOF-Based Magnetic Sponge System. *J. Am. Chem. Soc.* **2013**, *135*, 4040−4050.
(27) Dechambenoit, P.; Long, J. R. Microporous Magnets. *Chem. Soc. Rev.* **2011**, *40*, 3249−3265.
(28) Kresse, G.; Furthmuller, J. Efficiency of Ab-Initio Total Energy Calculations for Metals and Semiconductors Using a Plane-Wave Basis Set. *Comput. Mater. Sci.* **1996**, *6*, 15−50.
(29) Hammer, B.; Hansen, L.; Norskov, J. Improved Adsorption Energetics within Density-Functional Theory Using Revised Perdew−Burke−Ernzerhof Functionals. *Phys. Rev. B* **1999**, *59*, 7413−7421.
(30) Grimme, S. Semiempirical GGA-Type Density Functional Constructed with a Long-Range Dispersion Correction. *J. Comput. Chem.* **2006**, *16*, 1787−1799.
(31) Blochl, P. E. Projector Augmented-Wave Method. *Phys. Rev. B* **1994**, *50*, 17953−17979.
(32) Momma, K.; Izumi, F. VESTA: A Three-Dimensional Visualization System for Electronic and Structural Analysis. *J. Appl. Crystallogr.* **2008**, *41*, 653−658.
(33) Goodenough, J. Direct Cation−Cation Interactions in Several Oxides. *Phys. Rev.* **1960**, *117*, 1442−1451.
(34) Goodenough, J. B. *Magnetism and the Chemical Bond*; John Wiley & Sons, Inc.: New York; 1963.
(35) Canepa, P.; Chabal, Y. J.; Thonhauser, T. When Metal Organic Frameworks Turn into Linear Magnets. *Phys. Rev. B* **2013**, *87*, 094407.
(36) Miller, J. S.; Epstein, A. J. Organic and Organometallic Molecular Magnetic Materials − Designer Magnets. *Angew. Chem., Int. Ed.* **1994**, *33*, 385−415.